arXiv:1604.00092v1 [cs.CV] 1 Apr 2016

Variational reaction-diffusion systems for semantic segmentation

Paul Vernaza
NEC Laboratories America
10080 N. Wolfe Road, Cupertino, CA 95014
<pvernaza@nec-labs.com>

January 11, 2022

Abstract

A novel global energy model for multi-class semantic image segmentation is proposed that admits very efficient exact inference and derivative calculations for learning. Inference in this model is equivalent to MAP inference in a particular kind of vector-valued Gaussian Markov random field, and ultimately reduces to solving a linear system of linear PDEs known as a reaction-diffusion system. Solving this system can be achieved in time scaling near-linearly in the number of image pixels by reducing it to sequential FFTs, after a linear change of basis. The efficiency and differentiability of the model make it especially well-suited for integration with convolutional neural networks, even allowing it to be used in interior, feature-generating layers and stacked multiple times. Experimental results are shown demonstrating that the model can be employed profitably in conjunction with different convolutional net architectures, and that doing so compares favorably to joint training of a fully-connected CRF with a convolutional net.

1 Introduction

The focus of this work is the semantic segmentation problem, in which a learning system must be trained to predict a semantic label for each pixel of an input image. Recent advances in deep convolutional neural nets (CNNs), along with historical successes of global energy methods such as Conditional Random Fields (CRFs), have raised the natural question of how these methods might best be combined to achieve better results on difficult semantic segmentation problems. Although several proposals have recently emerged in this vein [2, 21, 16, 12], there is currently no clear consensus on how best to integrate these methods.

Achieving tighter integration between and better joint training of global energy models and CNNs is the key motivator for this work. To that end, this paper proposes a novel global energy model for semantic segmentation, referred to here as Variational Reaction Diffusion (or VRD). VRD can be thought of as a vector-valued Gaussian Markov Random Field (GMRF) model over a continuous domain (as opposed to

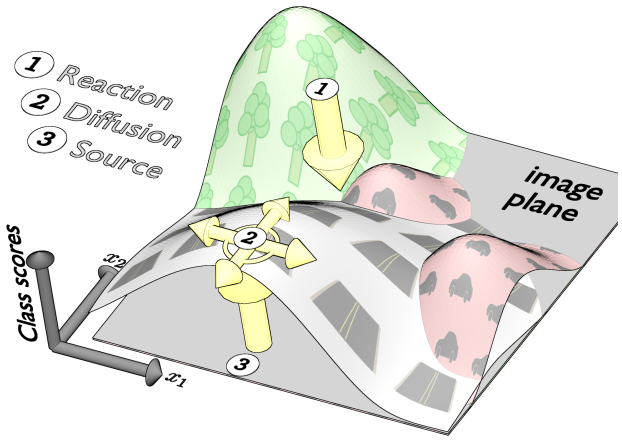


Figure 1: Illustration of reaction-diffusion analogy for an image segmentation task with three classes: road, tree, and car.

a graph). Unlike most other energy-based methods, *exact* inference in VRD can be performed very efficiently by reducing the problem to sequential FFTs, after a linear change of basis. Backpropagation and parameter derivatives can also be computed efficiently, making it an attractive choice for integration with CNNs. The efficiency of VRD also raises some interesting new possibilities for tight integration of CNNs with global energy methods: instead of appending a relatively complex CRF model to an existing CNN architecture, VRD may actually be used as an internal, feature-generating layer, for example. This possibility is explored in the experiments.

Since inference in VRD is linear in the inputs, an obvious concern is whether such a simple model manages to capture the most important features of seemingly more complex models requiring approximate inference or sophisticated combinatorial optimization. Although the possibility of layering somewhat negates this concern, Section 3 also provides some insight into this issue by showing how VRD can be considered a relaxation of other popular models. Experiments in Section 6 also shed some light on this question by showing that VRD compares favorably to more complex energy-based methods.

The name of the proposed method is a reference to the reaction-diffusion systems that initially inspired this work. Briefly, inference in VRD may be interpreted as evolving evidence (or class scores) under the dynamics of a reaction-diffusion process, as illustrated in Fig. 1. Intuitively, we might think of modeling evidence for one semantic class as being created by unary potentials (or the previous layer in a CNN), propagating across the image via diffusion, and reacting with evidence for other semantic classes. Each of these processes may locally create or suppress evidence for each class, and if we allow this process to reach an equilibrium, the sum of these effects must cancel at every point in the image (c.f. Eq. 2). By restricting the model to the class of such processes generating the solutions to convex, variational problems, we are essentially ensuring that such an equilibrium exists and is globally stable.

The rest of this paper is structured as follows. The next section gives a very brief overview of the method and a summary of the results that make inference and learning tractable. Section 3 motivates the model by comparing it to existing models, gives some intuition as to how inference works, and discusses other practical issues. The main results for inference and learning VRD are derived in Section 4. This is followed by a discussion of related work and experimental results.

2 Method overview

This section gives a brief overview of the main ideas and results of the method. Details will be discussed subsequently.

2.1 The model

Let $I \subset \mathbb{R}^2$ denote the image plane: i.e., a rectangular subset of $\mathbb{R}^2$ representing the domain of the image. VRD is given a spatially-varying set of N_i input features, represented here as a function $s^i : I \to \mathbb{R}^{N_i}$, and produces a set of N_o output scores $s^o : I \to \mathbb{R}^{N_o}$. For now, N_o might be thought of as the number of semantic classes, and we might think of $s^o_k(x)$ as a score associated with the kth class at $x \in I$, with a prediction generated via $\arg\max_k s^o_k(x)$. Throughout this paper, x will represent an arbitrary point in I.

Let $s = \begin{pmatrix} s^{o\mathsf{T}} & s^{i\mathsf{T}} \end{pmatrix}^\mathsf{T}$ denote the concatenation of s^i and s^o into a single function $I \to \mathbb{R}^{N_i+N_o}$. VRD generates s^o by solving the following optimization problem. In the following, the dependence of s on x has been omitted for clarity.

$$\arg\min_{s^o} \int_I s^\mathsf{T} Q s + \sum_{k=1}^{2} \frac{\partial s}{\partial x_k}^\mathsf{T} B \frac{\partial s}{\partial x_k} \,\mathrm{d}x. \tag{1}$$

Here, B and Q are assumed to be constant (i.e., independent of x) positive-definite parameter matrices. This is then an infinite-dimensional, convex, quadratic optimization problem in s^o.

2.2 Inference

Just as the minimum of a convex, finite-dimensional quadratic function can be expressed as the solution to a linear system, the solution to this infinite-dimensional quadratic can be expressed as the solution to the following linear system of PDEs:

$$B^o \Delta s^o - Q^o s^o = Q^i s^i - B^i \Delta s^i, \tag{2}$$

where the dependence on x has again been omitted, Δ represents the vector Laplacian ($(\Delta f)_i := \sum_j \frac{\partial^2 f_i}{\partial x_j^2}$), and B and Q have been partitioned into submatrices B^o, Q^o, B^i, and Q^i such that $s^\mathsf{T} Q s = s^{o\mathsf{T}} Q^o s^o + 2 s^{o\mathsf{T}} Q^i s^i + f(s^i)$ (and likewise for B). We can solve this system efficiently via a linear change of variables and a backsubstitution

procedure exactly analogous to the finite-dimensional case. Specifically, we first use the Schur decomposition to write $(B^o)^{-1}Q^o = VUV^\mathsf{T}$, where V is orthonormal and U is upper-triangular. We then perform the change of variables $z = V^\mathsf{T}s^o$. Let $s^p := Q^i s^i - B^i \Delta s^i$. We then solve for z via backsubstitution, first solving the following scalar PDE for z_{N_o}, fixing it, solving for z_{N_o-1}, and proceeding thus backwards to z_1:

$$\Delta z_k - U_{kk} z_k = (V^\mathsf{T}(B^o)^{-1}s^p)_k + \sum_{j=k+1}^{N_o} U_{kj} z_j. \tag{3}$$

After solving for z, the output scores are obtained via $s^o = Vz$. The scalar PDEs above may be discretized and solved either via the FFT or the multigrid method [1]. If L lattice points are used in the discretization, the total computational cost of solving (1) via FFT-based inference is $O({N_o}^3 + {N_o}^2 L + N_o L \log L + N_o N_i L)$.

2.3 Learning

In order to learn the model, we assume some arbitrary, differentiable loss $L(s^o)$ has been defined on the output scores s^o. Gradient-based learning is enabled by computing the derivatives of L with respect to the parameter matrices B, Q, and potentially the inputs s^i, allowing the model to be used in backpropagation.

The backpropagation derivative $\frac{\mathrm{d}L}{\mathrm{d}s^p} : I \to \mathbb{R}^{N_o}$ (with s^p defined as above) can be computed by solving the same PDE system (2) as in the inference step, but replacing s^p with $\frac{\mathrm{d}L}{\mathrm{d}s^o}$. Specifically, we solve

$$B^o \Delta \frac{\mathrm{d}L}{\mathrm{d}s^p} - Q^o \frac{\mathrm{d}L}{\mathrm{d}s^p} = \frac{\mathrm{d}L}{\mathrm{d}s^o} \tag{4}$$

for $\frac{\mathrm{d}L}{\mathrm{d}s^p}$, given $\frac{\mathrm{d}L}{\mathrm{d}s^o} : I \to \mathbb{R}^{N_o}$, in the same way as in the inference step. The parameter derivatives can be expressed as simple functions of the backpropagation derivative. These are as follows:

$$\frac{\mathrm{d}L}{\mathrm{d}B^o_{ij}} = -\left\langle \frac{\mathrm{d}L}{\mathrm{d}s^p_i}, \Delta s^o_j \right\rangle \tag{5}$$

$$\frac{\mathrm{d}L}{\mathrm{d}Q^o_{ij}} = \left\langle \frac{\mathrm{d}L}{\mathrm{d}s^p_i}, s^o_j \right\rangle, \tag{6}$$

where the inner product is defined in the standard way, as $\langle f, g \rangle := \int_I f(x)g(x)\,\mathrm{d}x$, and s^o is that computed via inference for the current values of B and Q.

3 Analysis

3.1 Comparison to other energy-based models

Although the model (1) may appear quite different from other energy-based models due to the continuous formulation, the motivation for and structure of the model is

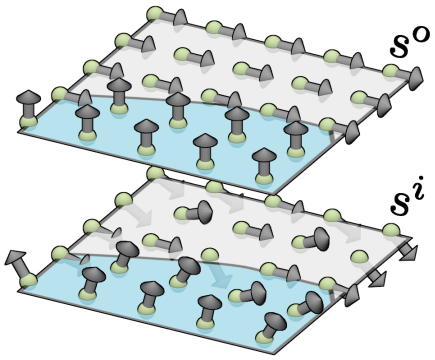


Figure 2: Illustration of variational model. Fig. 2 depicts the discretized model: at each grid location (green ball), we are given an input vector (arrows on lower plane). For appropriate choice of Q, input vectors s^i can be thought of as noisy estimates of output vectors s^o, which are to be inferred. Blue-shaded area represents one class, while white area represents other class. Learning essentially trains output arrows in blue area to point upwards and arrows in white area to point to the right.

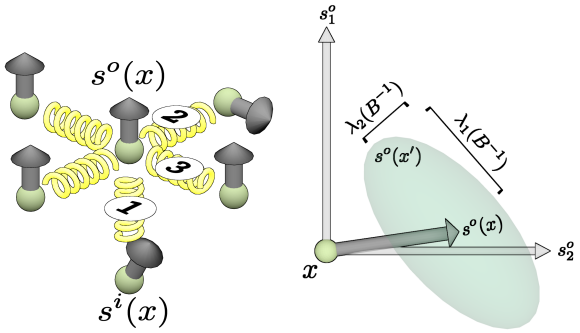
very similar to that for more familiar models. A typical CRF model for segmentation represents a distribution over (class-label-valued) functions defined on the nodes of a graph, which represent pixels or regions. Inference using the mean-field approximation reduces to finding a simplex-valued function on the graph (representing the pseudo-marginal label distributions), subject to some local self-consistency conditions. Unary potentials serve to anchor the distributions at each point, while binary potentials encourage smoothness of these distributions with respect to neighboring points.

By contrast, VRD produces a vector-valued score function defined on I. The derivatives in (1) can be replaced by finite-difference approximations to obtain a model defined over a regular lattice graph. This is illustrated in Fig. 2. Unary and binary potentials are both quadratic, as illustrated in Fig. 3a. Since all the potentials are quadratic, the overall energy of (1) can be thought of as the unnormalized log-likelihood of a Gaussian Markov random field, albeit a vector-valued variant.

It is therefore evident that the principal difference between the mean-field CRF and VRD models is that VRD relaxes the probability simplex constraints on its outputs, and instead produces unnormalized score functions. VRD also assumes the additional structure that the domain of the modeled function must be equivalent to Euclidean space, and the unary and binary potentials must be quadratic. These key assumptions enable very efficient, exact inference.

3.2 Motivation for binary potential

The quadratic binary potential in (1) can be thought of as a natural extension of the standard Potts model commonly employed in energy-based methods. To make this clear, consider a finite-difference approximation of the quadratic term in (1). Denoting



(a) (b)

Figure 3: Fig. 3a: depiction of quadratic unary and binary potentials. Spring marked (1) corresponds to unary term $s^\mathsf{T} Q s$, spring marked (2) corresponds to binary term $\frac{\partial s}{\partial x_2}^\mathsf{T} B \frac{\partial s}{\partial x_2}$, and spring marked (3) corresponds to binary term $\frac{\partial s}{\partial x_1}^\mathsf{T} B \frac{\partial s}{\partial x_1}$. Fig. 3b: illustration of (log) Gaussian form of binary potential. For each location x, the potential is high when neighboring vector $s^o(x')$ is outside an ellipse centered at $s^o(x)$ with axes determined by B.

by δ_k a unit vector aligned to axis k, we have

$$\frac{\partial s^o}{\partial x_k}^\mathsf{T} B \frac{\partial s^o}{\partial x_k} \approx \epsilon^{-2} \|s^o(x + \epsilon\delta_k) - s^o(x)\|_B^2, \tag{7}$$

where ϵ is a small step size. If s^o were a binary indicator vector ($s_j^o(x) = 1 \iff \text{label}(x) = j$), and we had $B = I$, then this term would correspond exactly to the Potts potential $\mathbb{1}\{\text{label}(x) \neq \text{label}(x + \epsilon\delta_k)\}$. Fig. 3b illustrates the effect of the binary potential for the general case: it essentially serves as a Gaussian prior on the difference between score vectors of neighboring points.

3.3 Comparison with submodular combinatorial optimization

Here it is shown that the assumption of convexity of (1) is akin to the common assumption of submodular potentials in combinatorial global energy models. In particular, it is demonstrated that in the binary-label case, a discretized special case of (1) corresponds to a continuous relaxation of a binary, submodular optimization problem.

Fixing $Q^o = I$, $Q^i = -I$, $B^i = 0$, discretizing (1) via finite differences, and defining an appropriate lattice graph with ϵ-spaced nodes $\mathcal{N}$ and edges $\mathcal{E}$ yields

$$\begin{aligned} \arg\min_{s^o} \sum_{x \in \mathcal{N}} & \|s^o(x)\|^2 - 2 s^o(x)^\mathsf{T} s^i(x) \\ & + \sum_{(x,x') \in \mathcal{E}} \epsilon^{-2} \|s^o(x') - s^o(x)\|_{B^o}^2. \end{aligned} \tag{8}$$

An analogous combinatorial optimization can be defined by optimizing over binary indicator vectors instead of s^o. Let $\mathbf{1}_j \in \{0,1\}^{N_o}$ denote the vector that is 1 in the jth position and 0 elsewhere. The analogous combinatorial optimization is then

$$\arg\min_{l} \sum_{x \in \mathcal{N}} \|\mathbf{1}_{l(x)}\|^2 - 2\mathbf{1}_{l(x)}^{\mathsf{T}} s^i(x) + \sum_{(x,x') \in \mathcal{E}} \epsilon^{-2} \|\mathbf{1}_{l(x')} - \mathbf{1}_{l(x)}\|_{B^o}^2. \tag{9}$$

The term $E_b(i,j) := \|\mathbf{1}_i - \mathbf{1}_j\|_{B^o}^2$ is referred to as the binary potential. In the binary-label case ($N_o = 2$), this optimization is said to be submodular if the following condition holds:

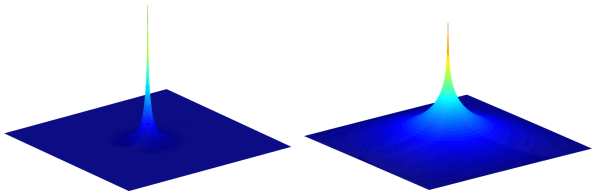
$$E_b(0,0) + E_b(1,1) \leq E_b(0,1) + E_b(1,0). \tag{10}$$

In our case, we have $E_b(0,0) = E_b(1,1) = 0$ and $E_b(1,0) = E_b(0,1) = B_{00}^o + B_{11}^o - B_{10}^o - B_{01}^o$, which is nonnegative by the convexity assumption, since convexity requires that B^o be positive semidefinite. This implies that the combinatorial analog of (8) is submodular in the binary-label case. Equivalently, we may interpret (8) as a relaxation of a combinatorial optimiziation obtained by relaxing the integrality and simplex constraints on s^o. This may also be compared to LP relaxation, which would relax the integrality constraint, but retain the simplex constraints, at the expense of harder optimization.

3.4 Intuition for inference

The key step in performing inference is the solution of the scalar PDEs (3). In the case of constant B and Q, this can be solved by taking the Fourier transform of both sides, solving algebraically for the transform of the solution, and then inverting the transform. This process is equivalent to convolving the right-hand side in the spatial domain with the *Green's function*, which is illustrated in Fig. 4. It is therefore evident that for large values of U_{kk}, solving (3) essentially convolves the right-hand side with a delta function (i.e., applying the identity function), while the solution for small values of U_{kk} convolves the right-hand side with an edge-preserving filter with a very wide support. Recalling that the U_{kk} are the (positive) eigenvalues of $(B^o)^{-1}Q^o$, it is also therefore evident that the amount of smoothing scales with the scale of B^o and inversely with the scale of Q^o. Intuitively, this means that the smoothing decreases as the unary penalty grows and increases as the binary penalty grows, just as one might expect.

In practice, (3) is solved via discretization and discrete Fourier transforms. Specifically, the right-hand side of (3) is discretized over a regular grid, and the goal is then to obtain samples of z_{kk} over the same grid. To do this, the Laplacian is first discretized in the usual way. Letting f denote the right-hand side of (3), assuming I has been discretized such that (x_i, y_j) represents the (i,j)th grid point, and assuming unit distance between adjacent grid points, this yields the following finite system of linear equations



(a) $U_{kk} = 10^{-2}$ (b) $U_{kk} = 10^{-6}$

Figure 4: The Green's function for the scalar PDE (3), for varying values of U_{kk}. The PDE can be solved by convolving the right-hand side with this function.

$\forall (i, j)$:

$$f(x_i, y_j) = -(U_{kk} + 4) z_{kk}(x_i, y_j) + \sum_{\|\delta\|_1 = 1, \delta \in \mathbb{Z}^2} z_{kk}(x_{i+\delta_1}, y_{j+\delta_2}). \tag{11}$$

Assuming zero boundary conditions, this system can be solved by a discrete sine transform. Since the above expression can be written as a convolution of z_{kk} with some filter F, this is a deconvolution problem to find z_{kk} given f, and it can be solved by the aforementioned transform, multiply, inverse-transform method.

3.5 Reparameterization

In practice, it was found that a naive parameterization of B and Q caused optimization problems in learning due to ill-conditioning. Figure 4 hints at the reason for this: the amount of smoothing varies dramatically as the eigenvalues of $(B^o)^{-1} Q^o$ vary in a very small region around zero. An exponential change of coordinates helps to remedy this situation. Specifically, matrices $\bar{B}^o$ and $\bar{Q}^o$ are defined such that $B^o = \exp \bar{B}^o$ and $Q^o = \exp \bar{Q}^o$, where exp refers to the matrix exponential. The learning optimization is then performed in the variables $\bar{B}^o$ and $\bar{Q}^o$.

The loss derivatives with respect to the new variables can be computed as follows. Define $\frac{\mathrm{d}L}{\mathrm{d}Q^o}$ as in (6). Let $\bar{Q}^o = U \Lambda U^\mathsf{T}$ be an eigendecomposition of $\bar{Q}^o$, defining U and Λ. Then, using known results for the derivative of the matrix exponential [14], it can be shown that

$$\frac{\mathrm{d}L}{\mathrm{d}\bar{Q}^o} = U \left(\left(U^\mathsf{T} \frac{\mathrm{d}L}{\mathrm{d}Q^o}^\mathsf{T} U \right) \odot \Phi \right) U^\mathsf{T}, \tag{12}$$

where $\odot$ is the Hadamard (elementwise) product and Φ is defined as follows (defining $\lambda_i := \Lambda_{ii}$):

$$\Phi_{ij} = \begin{cases} (e^{\lambda_i} - e^{\lambda_j})/(\lambda_i - \lambda_j) & \text{if } \lambda_i \neq \lambda_j \\ e^{\lambda_i} & \text{if } \lambda_i = \lambda_j \end{cases}. \tag{13}$$

For the above to hold, and for Q^o to be positive definite, $\bar{Q}^o$ must also be symmetric. This can be enforced by a final transformation, representing $\bar{Q}^o$ as the sum of another

matrix and its transpose. It is then straightforward to apply the chain rule to find the derivative with respect to that parameterization. The expression for $\frac{\mathrm{d}L}{\mathrm{d}B^o}$ is analogous to (12).

3.6 Computational complexity

Computationally, inference can be decomposed into three components: performing the Schur decomposition, performing a change of basis, and solving the scalar PDEs via backsubstitution. The cost of performing the Schur decomposition is $O({N_o}^3)$ [7]. Let L denote the total number of points in the lattice discretization (i.e., the number of pixels in the image). The change of basis $z = V^{\mathsf{T}} s^o$ (and its inverse) consists of transforming a N_o-dimensional vector via the square matrix V at each lattice point, at a cost of $O({N_o}^2 L)$. The backsubstitution procedure (3) consists of computing the right-hand side, which costs $O({N_o}^2 L)$, and solving the N_o scalar PDEs. Solving each via the DST costs $O(L \log L)$. Comptuing s^p costs an additional $O(N_o N_i L)$. The total computational complexity of inference is therefore $O({N_o}^3 + {N_o}^2 L + N_o L \log L + N_o N_i L)$. Computing the derivatives for learning requires the same amount of work, plus an additional $O(L)$ work to compute each component of (6) and (5). The asymptotic complexity is therefore the same as for inference.

4 Derivation

The results of Section 2 are now derived.

4.1 Deriving the reaction-diffusion PDE

First, the convexity of (1) is easily shown under the assumption of positive-semidefiniteness of B and Q (by showing Jensen's inequality holds—proof omitted). This implies that any stationary point of (1) must be optimal. We can find a stationary point by first finding the linear part of (1) for small variations (i.e., the Fréchet derivative) and then equating this to zero. Denote by $J : C^2(\mathbb{R}^2; \mathbb{R}^{N_i+N_o}) \to \mathbb{R}$ the objective function in (1), which maps a twice-differentiable, vector-valued function on $\mathbb{R}^2$ to a scalar. Let the notation $\mathrm{d}f_x$ represent the derivative of a function f at a point x, so that $\mathrm{d}J_s : C^2(\mathbb{R}^2; \mathbb{R}^{N_i+N_o}) \to \mathbb{R}$ represents the derivative of J at s. $\mathrm{d}J_s$ is identified as the coefficient of ϵ in $J(s + \epsilon v)$, where v is an arbitrary variation. This yields

$$\mathrm{d}J_s(v) = 2 \int_I v^{\mathsf{T}} Q s + \sum_{k=1}^{2} \frac{\partial v}{\partial x_k}^{\mathsf{T}} B \frac{\partial s}{\partial x_k} \, \mathrm{d}x, \tag{14}$$

which is verified to be the derivative, as it is linear in v. We now wish to express the term involving B as an inner product with v. To do so, we first rewrite this term (dropping the 2) as

$$\int_I \sum_{i,j=1}^{N_i+N_o} \nabla v_i^{\mathsf{T}} \nabla s_j B_{ij} \, \mathrm{d}x. \tag{15}$$

We then apply Green's identity

$$\int_I \psi \Delta \phi + \nabla \psi^\mathsf{T} \nabla \phi \, \mathrm{d}x = \int_{\partial I} \psi \nabla \phi^\mathsf{T} \hat{n} \, \mathrm{d}S \tag{16}$$

for $\phi = v_i$, $\psi = s_j$, use the fact that $v_i = 0$ on ∂I, and regroup terms to obtain

$$\mathrm{d}J_s(v) = 2 \int_I v^\mathsf{T} (Qs - B\Delta s) \, \mathrm{d}x. \tag{17}$$

Stationarity requires that this be zero on the subspace of feasible variations, which consists of those variations that do not change the s^i components, as these are assumed fixed. Decomposing v as $v = \begin{pmatrix} v^{o\mathsf{T}} & v^{i\mathsf{T}} \end{pmatrix}^\mathsf{T}$, we have $v^i = 0$ and

$$\int_I v^{o\mathsf{T}} (Q^o s^o + Q^i s^i - B^o \Delta s^o - B^i \Delta s^i) \, \mathrm{d}x = 0. \tag{18}$$

Finally, applying the fundamental lemma of the calculus of variations yields (2).

4.2 Solving the PDE system

The next step is to reduce the solution of (2) to a sequence of scalar PDE subproblems. Again defining $s^p = Q^i s^i - B^i \Delta s^i$, we left-multiply (2) by $(B^o)^{-1}$ to obtain

$$\Delta s^o - (B^o)^{-1} Q^o s^o = (B^o)^{-1} s^p. \tag{19}$$

We then use the Schur decomposition [7] to write $(B^o)^{-1} Q^o = V U V^\mathsf{T}$, where V is orthonormal. The assumption that B and Q are positive-definite implies that B^o and Q^o are also positive definite, which implies that $(B^o)^{-1} Q^o$ has a complete set of real, positive eigenvalues (equal to those of $\sqrt{B^o} Q^o \sqrt{B^o}$, which is positive-definite). By the properties of the Schur decomposition, U will therefore be upper-triangular, with the positive eigenvalues of $(B^o)^{-1} Q^o$ on the diagonal. Substituting the Schur decompsition and left-multiplying by V^T yields

$$V^\mathsf{T} \Delta s^o - U V^\mathsf{T} s^o = V^\mathsf{T} (B^o)^{-1} s^p. \tag{20}$$

The next, key step is to observe that the vector Laplacian commutes with constant linear transformations: i.e., $V^\mathsf{T} \Delta s^o = \Delta V^\mathsf{T} s^o$. This is straightforward to show by expanding the definitions of matrix multiplication and the vector Laplacian. This allows us to perform the change of coordinates $z = V^\mathsf{T} s^o$, and to solve for z instead. The fact that U is upper-triangular allows us to solve for z via the backsubstitution algorithm in (3).

4.3 Derivatives

Inference is regarded as a function mapping s^p (as previously defined) to s^o by solving (2). The fact that this function is well-defined follows from the uniqueness of solutions of (2), which follows from the assumption that B and Q are positive definite, and the fact that the scalar PDEs (3) have unique solutions [5]; in other words, the

linear differential operator $B^o\Delta - Q^o$ is invertible. Let $G := (B^o\Delta - Q^o)^{-1}$. We now assume a loss L is defined on the output of G, and we wish to find the derivatives of the loss with respect to the input of G (i.e., the backpropagation derivative) as well as the derivatives with respect to the parameters B^o and Q^o.

First, we assume that the derivative of L is provided in the form of a function $\frac{\mathrm{d}L}{\mathrm{d}s^o} : I \to \mathbb{R}^{N_o}$:

$$(\mathrm{d}L_{s^o})v = \left\langle \frac{\mathrm{d}L}{\mathrm{d}s^o}, v \right\rangle, \tag{21}$$

where v is an arbitrary variation. Intuitively, $\frac{\mathrm{d}L}{\mathrm{d}s^o}$ represents the differential change in L due to a variation of s^o at the point given by its input. We would like to obtain the derivative of $L \circ G$ in the same form. By the chain rule and the definition of the adjoint,

$$\begin{aligned}(\mathrm{d}(L \circ G)_{s^p})v &= \left\langle \frac{\mathrm{d}L}{\mathrm{d}s^o}, (\mathrm{d}G_{s^p})v \right\rangle \\ &= \left\langle (\mathrm{d}G_{s^p})^* \frac{\mathrm{d}L}{\mathrm{d}s^o}, v \right\rangle. \end{aligned} \tag{22}$$

Since G is linear in s^p, $\mathrm{d}G_{s^p} = G$. Furthermore, G is self-adjoint; this follows from the fact that $B^o\Delta - Q^o$ is self-adjoint, which in turn can be shown given that B^o and Q^o are self-adjoint (by the assumption of positive-definiteness) and B^o commutes with Δ. This implies $\frac{\mathrm{d}L}{\mathrm{d}s^p} = G\frac{\mathrm{d}L}{\mathrm{d}s^o}$, which is equivalent to (4).

To obtain the parameter derivatives, we directly consider the effect of adding a small perturbation to each parameter. We first define the unperturbed solution s^o as the solution to $(B^o\Delta - Q^o)s^o = s^p$, given the input s^p. We then define the perturbed solution $\tilde{s}^o$ as the solution to $((B^o + \epsilon V)\Delta - Q^o)\tilde{s}^o = s^p$, where ϵV is a variation of B^o. We then find the following expansion of $\tilde{s}^o$ in ϵ. In the following, the notation G_{B^o} is used to refer to G evaluated with the parameter B^o.

$$\begin{aligned}(B^o\Delta - Q^o)\tilde{s}^o &= s^p - \epsilon V\Delta\tilde{s}^o \\ \tilde{s}^o &= G_{B^o}(s^p - \epsilon V\Delta\tilde{s}^o) \\ &= s^o - \epsilon G_{B^o}V\Delta\tilde{s}^o \\ &= s^o - \epsilon G_{B^o}V\Delta(s^o - \epsilon G_{B^o}V\Delta\tilde{s}^o) \\ &= s^o - \epsilon G_{B^o}V\Delta s^o + O(\epsilon^2) \end{aligned} \tag{23}$$

Note that the preceding two lines are obtained by recursive expansion. This implies that $(\mathrm{d}G_{B^o})V = -G_{B^o}V\Delta s^o$, again abusing notation so that $\mathrm{d}G_{B^o}$ refers to the derivative of G as a function of the parameter B^o, and evaluated at the point B^o. The chain rule and adjoint property are applied again to obtain

$$(\mathrm{d}(L \circ G)_{B^o})V = \left\langle -G_{B^o}\frac{\mathrm{d}L}{\mathrm{d}s^o}, V\Delta s^o \right\rangle \tag{24}$$

$$= \left\langle -\frac{\mathrm{d}L}{\mathrm{d}s^p}, V\Delta s^o \right\rangle. \tag{25}$$

The previous arguments apply even in the case that B^o is a function of I (i.e., depends on x). If B^o is constrained to be constant on I, however, the variations V must also be

constant, and we can write a basis for these in the form $\mathbf{1}_i\mathbf{1}_j^\mathsf{T}$, for $(i,j) \in \{1,\dots,N_o\}^2$. We then define $\frac{\mathrm{d}L}{\mathrm{d}B^o_{ij}} = (\mathrm{d}(L \circ G)_{B^o})\mathbf{1}_i\mathbf{1}_j^\mathsf{T}$. Evaluating this using the expression above then yields (5). Repeating the argument above *mutatis mutandis* for Q^o yields (6).

5 Related work

The method proposed here is comparable to recent work on joint training of CNNs and CRFs. In particular, [21] and [16] both propose backpropagation-through-inference techniques in order to jointly train fully-connected CRFs (FC-CRFs) [11] and CNNs. Inference consists of performing a fixed number of message-passing iterations on the pseudo-marginals of the mean-field approximation. These message-passing steps are then regarded as a formal composition of functions, to which backpropagation is applied. The FC-CRF model is probably more expressive than VRD, in that it features non-local connections. However, this comes at the expense of having to resort to approximate inference. The asymptotic complexity of performing a single message-passing round in the FC-CRF is comparable to that of completing the entire exact inference procedure in VRD. The method of [15] is also notable for jointly training a CNN with inference based on a global convex energy model, but inference and learning in this model rely on general optimization techniques that are costly when dealing with image-sized optimization problems.

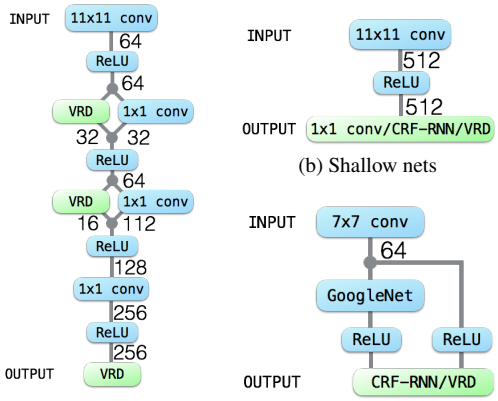
Gaussian random field models have previously been applied to the task of semantic segmentation [20] and related tasks [19, 9]; however, exact inference in these methods scales at least quadratically in the number of pixels, making approximate inference necessary again.

Recent work [3] learned reaction-diffusion processes for image restoration; however, this work relied on simulating the process in time to do inference and learning, resulting in a method very similar to the aforementioned backpropagation-through-inference techniques.

Solving the PDE (2) is related to Wiener filtering. It is known that certain *scalar-valued* Gaussian MRFs may be solved via Wiener filtering [18]; to our knowledge, the inference procedure in this work is novel in that it essentially reduces inference in a *vector-valued* Gaussian MRF to repeated Wiener filtering.

6 Experiments

VRD was implemented in Caffe [10] and compared to several other methods on two datasets: the KITTI road segmentation dataset [6] (a binary classification problem) and the Stanford background dataset [8] (an 8-way classification problem). The experiments were conducted with the following primary goals in mind: (1) to directly compare VRD to an global energy method based on "backpropagation-through-approximate-inference;" (2) to investigate whether composing multiple VRD layers is feasible and/or beneficial; and (3) to see whether integration of VRD with deep CNNs might provide any benefit.



(a) Layered VRD (b) Shallow nets (c) GoogleNet + CRF/VRD

Figure 5: Architectures used in experiments. Numbers under layers indicate number of output channels produced.

All of the parameters (CRF, VRD, and convolution) in all of the experiments were trained jointly via backpropagation, using the AdaGrad algorithm [4]. Each experiment consisted of training all parameters from scratch—i.e., using random initialization and no other training data besides—and all experiments were run until the loss converged (using a stepwise-annealed learning rate). The softmax loss was used for all experiments. VRD was compared to the previously discussed method of [21], referred to here as CRF-RNN, which performs backpropagation through approximate inference for a FC-CRF. The default number of mean-field iterations (10) was used for this method. The authors' public implementation was used. The method of [17], referred to here as GoogleNet, was also evaluated. The public BVLC implementation was used, slightly modified for semantic segmentation by transforming it into a fully-convolutional model [13]. A single random split of each dataset was chosen, with 80% of the data reserved for training and the remaining held-out. Each experiment reports the results of evaluation on this held-out set.

Each experiment involved training a CNN with one of three general architectures, which are illustrated in Fig. 5. Each type of architecture was designed primarily with the goal of testing one of the questions mentioned above. Experiments with shallow architectures were designed to directly compare the merits of different global energy models. The *Layered VRD* experiments were intended to test whether layering VRD layers is feasible and provides any benefit (the *layered baseline* experiment is identical to Layered VRD, but exchanging the VRD layers with 1x1 convolutions). The *GoogleNet* experiments were intended to test whether VRD is useful in the context of joint training with a deep CNN.

Precision-recall curves for the KITTI experiments are shown in Fig. 7, and qualitative results are shown in Fig. 6. Table 1 lists evaluation results for both datasets: for KITTI, maximum F1 and AP are reported in the birds-eye view (as suggested in [6]); and for Stanford Background (abbreviated SBG), pixel-level accuracies are reported.

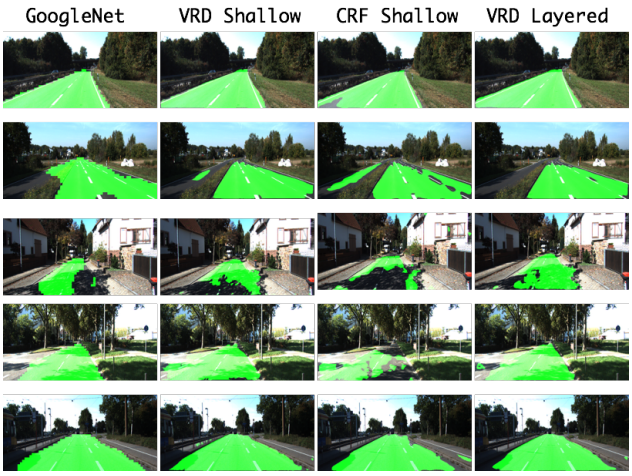


Figure 6: Qualitative results for KITTI dataset.

	KITTI		SBG
Method	Max F1	AP	Acc.
Shallow CNN	82.84	88.29	56.1
Shallow CRF-RNN	86.14	90.64	59.3
Shallow VRD	88.22	91.76	62.7
GoogleNet	**88.62**	91.25	65.0
GoogleNet + CRF-RNN	87.72	91.49	68.2
GoogleNet + VRD	88.07	91.38	**70.7**
Layered baseline	82.55	88.56	55.2
Layered VRD	88.58	**92.14**	61.5

Table 1: Experimental results

Comparing VRD and CRF-RNN, it was consistently observed that better results were obtained using VRD. The most significant benefits were observed with shallow architectures, although a significant benefit was also observed in the experiments with GoogleNet on SBG. Layering VRD proved to be both practical and beneficial. On the KITTI dataset, this method seemed to produce the best overall results, despite having far fewer parameters and a far simpler architecture than GoogleNet. However, this architecture had too few parameters to fit the SBG data well. Finally, joint training of VRD with GoogleNet was not beneficial for the KITTI dataset; however, a large benefit was seen on the more difficult SBG dataset.

To give a general idea of the computational efficiency of VRD, for an internal VRD layer with $N_i = 64$, $N_o = 32$, and an image size of 511x255 ($L = 130305$), forward-pass inference took 408 ms, and computing derivatives in the backwards pass took 760 ms. These timings are for a CPU implementation, although s^p was computed via GPU convolutions.

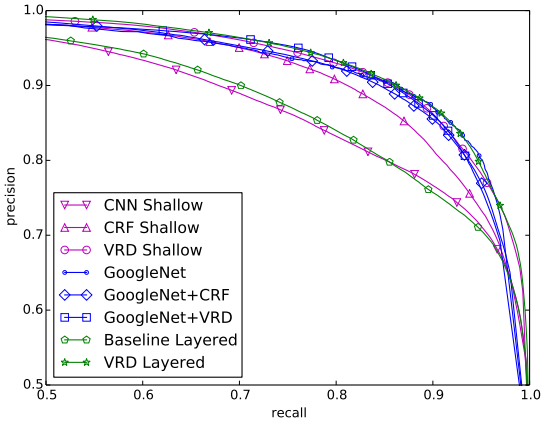


Figure 7: Precision-recall curves for KITTI experiments.

7 Conclusions

A global energy model for semantic segmentation featuring very efficient exact inference was proposed. Inference in VRD for a problem with N_o output labels reduces to a sequence of N_o convolutions, which can be implemented efficiently via the FFT, and backpropagation and parameter derivatives for learning can be computed just as efficiently, making it an attractive choice for joint training with CNNs.

Analysis revealed how VRD can be thought of as a relaxation of other global energy methods. Despite this, experiments demonstrated superior performance of VRD compared to a more complex FC-CRF-based model in the context of joint training with a CNN. This suggests that, at least in the tested scenarios, the benefits of exact inference may outweigh those of having a more expressive or sophisticated model. The experiments also demonstrated the feasibility of composing multiple VRD layers, and this yielded promising results.

In the short term, more work needs to be done to devise and test CNN architectures that are able to leverage the ability of VRD to efficiently produce and backpropagate through exact global inferences. In the longer term, it is hoped that the insights developed here will lead to a better general understanding of how best to integrate CNNs with global energy models.

References

[1] Achi Brandt. Guide to multigrid development. In *Multigrid methods*, pages 220–312. Springer, 1982.

[2] Liang-Chieh Chen, George Papandreou, Iasonas Kokkinos, Kevin Murphy, and Alan L Yuille. Semantic image segmentation with deep convolutional nets and

fully connected crfs. In *ICLR*, 2015.

[3] Yunjin Chen, Wei Yu, and Thomas Pock. On learning optimized reaction diffusion processes for effective image restoration. In *Proceedings of the IEEE Conference on Computer Vision and Pattern Recognition*, pages 5261–5269, 2015.

[4] John Duchi, Elad Hazan, and Yoram Singer. Adaptive subgradient methods for online learning and stochastic optimization. *The Journal of Machine Learning Research*, 12:2121–2159, 2011.

[5] Lawrence C Evans. *Partial differential equations*. American Mathematical Society, 2010.

[6] Jannik Fritsch, Tobias Kuehnl, and Andreas Geiger. A new performance measure and evaluation benchmark for road detection algorithms. In *International Conference on Intelligent Transportation Systems (ITSC)*, 2013.

[7] Gene H Golub and Charles F Van Loan. *Matrix computations*, volume 3. JHU Press, 2012.

[8] Stephen Gould, Richard Fulton, and Daphne Koller. Decomposing a scene into geometric and semantically consistent regions. In *Computer Vision, 2009 IEEE 12th International Conference on*, pages 1–8. IEEE, 2009.

[9] Jeremy Jancsary, Sebastian Nowozin, Toby Sharp, and Carsten Rother. Regression tree fieldsan efficient, non-parametric approach to image labeling problems. In *Computer Vision and Pattern Recognition (CVPR), 2012 IEEE Conference on*, pages 2376–2383. IEEE, 2012.

[10] Yangqing Jia, Evan Shelhamer, Jeff Donahue, Sergey Karayev, Jonathan Long, Ross Girshick, Sergio Guadarrama, and Trevor Darrell. Caffe: Convolutional architecture for fast feature embedding. *arXiv preprint arXiv:1408.5093*, 2014.

[11] Philipp Krähenbühl and Vladlen Koltun. Efficient inference in fully connected crfs with gaussian edge potentials. In J. Shawe-Taylor, R.S. Zemel, P.L. Bartlett, F. Pereira, and K.Q. Weinberger, editors, *Advances in Neural Information Processing Systems 24*, pages 109–117. Curran Associates, Inc., 2011.

[12] Guosheng Lin, Chunhua Shen, Ian D. Reid, and Anton van den Hengel. Efficient piecewise training of deep structured models for semantic segmentation. *CoRR*, abs/1504.01013, 2015.

[13] Jonathan Long, Evan Shelhamer, and Trevor Darrell. Fully convolutional networks for semantic segmentation. In *Proceedings of the IEEE Conference on Computer Vision and Pattern Recognition*, pages 3431–3440, 2015.

[14] Igor Najfeld and Timothy F Havel. Derivatives of the matrix exponential and their computation. *Advances in Applied Mathematics*, 16(3):321–375, 1995.

[15] René Ranftl and Thomas Pock. A deep variational model for image segmentation. In *Pattern Recognition*, pages 107–118. Springer, 2014.

[16] Alexander G Schwing and Raquel Urtasun. Fully connected deep structured networks. *arXiv preprint arXiv:1503.02351*, 2015.

[17] Christian Szegedy, Wei Liu, Yangqing Jia, Pierre Sermanet, Scott Reed, Dragomir Anguelov, Dumitru Erhan, Vincent Vanhoucke, and Andrew Rabinovich. Going deeper with convolutions. *CoRR*, abs/1409.4842, 2014.

[18] Richard Szeliski. *Computer vision: algorithms and applications*. Springer Science & Business Media, 2010.

[19] Marshall F Tappen. Utilizing variational optimization to learn markov random fields. In *Computer Vision and Pattern Recognition, 2007. CVPR'07. IEEE Conference on*, pages 1–8. IEEE, 2007.

[20] Marshall F Tappen, Kegan GG Samuel, Craig V Dean, and David M Lyle. The logistic random fielda convenient graphical model for learning parameters for mrf-based labeling. In *Computer Vision and Pattern Recognition, 2008. CVPR 2008. IEEE Conference on*, pages 1–8. IEEE, 2008.

[21] Shuai Zheng, Sadeep Jayasumana, Bernardino Romera-Paredes, Vibhav Vineet, Zhizhong Su, Dalong Du, Chang Huang, and Philip HS Torr. Conditional random fields as recurrent neural networks. In *Proceedings of the IEEE International Conference on Computer Vision*, pages 1529–1537, 2015.